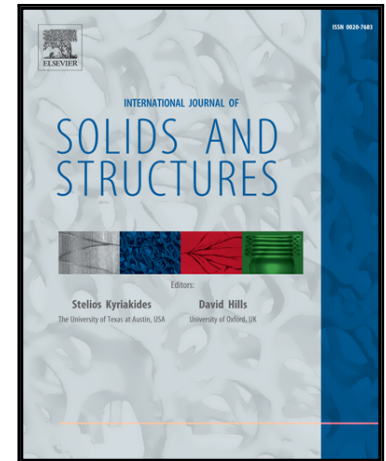


## Accepted Manuscript

One dimensional constitutive model with transformation surfaces for phase transition in shape memory alloys considering the effect of loading history

M. Shirani , M. Kadkhodaei

PII: S0020-7683(15)00481-3  
DOI: [10.1016/j.ijsolstr.2015.11.019](https://doi.org/10.1016/j.ijsolstr.2015.11.019)  
Reference: SAS 8970



To appear in: *International Journal of Solids and Structures*

Received date: 8 March 2014  
Revised date: 27 September 2015  
Accepted date: 25 November 2015

Please cite this article as: M. Shirani , M. Kadkhodaei , One dimensional constitutive model with transformation surfaces for phase transition in shape memory alloys considering the effect of loading history, *International Journal of Solids and Structures* (2015), doi: [10.1016/j.ijsolstr.2015.11.019](https://doi.org/10.1016/j.ijsolstr.2015.11.019)

This is a PDF file of an unedited manuscript that has been accepted for publication. As a service to our customers we are providing this early version of the manuscript. The manuscript will undergo copyediting, typesetting, and review of the resulting proof before it is published in its final form. Please note that during the production process errors may be discovered which could affect the content, and all legal disclaimers that apply to the journal pertain.

# One dimensional constitutive model with transformation surfaces for phase transition in shape memory alloys considering the effect of loading history

M. Shirani and M. Kadkhodaei<sup>1\*</sup>

Department of Mechanical Engineering, Isfahan University of Technology, Isfahan, 84156-83111, Iran

## Abstract

Existing constitutive models for Shape Memory Alloys (SMAs) assume that both forward and reverse transformations occur when the thermodynamic driving force reaches a specific amount regardless of loading history. In this article, these assumptions are examined, and some cases are introduced where these models predict contradictory results. The effects of initial martensitic volume fraction on both forward and reverse transformations are shown by carrying out simple tensile tests on SMA wires. In line with these experiments, a one-dimensional constitutive model with new transformation conditions is proposed phenomenologically in order to model pseudoelastic behavior. The constitutive model is proved to be consistent with the theory of continuum mechanics. New transformation surfaces are introduced to govern transformations start conditions, rather than using preexisting common phase diagrams. As a result, history-dependent transformation start temperatures are determined. The obtained experimental stress-strain diagrams, available DSC test results, and experimental strain-temperature responses are used to validate the proposed model. It is shown that loading history affects transformation start conditions.

**Key words:** shape memory alloys, pseudoelastic, constitutive model, phase diagram, transformation surface, loading history, history-dependent transformation temperature.

---

\*Corresponding author. Tel.: +98 31 33915256; fax: +98 31 33912628.  
E-mail address: [kadkhodaei@cc.iut.ac.ir](mailto:kadkhodaei@cc.iut.ac.ir) (M. Kadkhodaei)

## 1. Introduction

Shape Memory Alloys (SMAs) are a branch of smart materials that can return to their initial shape after being subjected to inelastic deformations. The mechanism underlying this property is based on a martensitic transformation between austenite and martensite phases. At zero stress, by heating, transformation from martensite to austenite begins at  $A_s$  (austenite start temperature) and ends at  $A_f$  (austenite final temperature). When austenite is cooled, transformation to martensite starts at  $M_s$  (martensite start temperature) and finishes at  $M_f$  (martensite final temperature). The obtained phase is called twinned martensite. If martensite is formed in the presence of stress, detwinned martensite along with macroscopic strains are obtained. This strain will disappear when the material is heated above  $A_f$ . This property is named Shape Memory Effect (SME) (Brinson 1993) since the material goes back to its initial configuration. At a constant temperature above  $A_f$ , during loading, austenite transforms to martensite but returns to its initial phase and shape in the course of unloading. This phenomenon is named Pseudoelasticity (PE) (Brinson 1993). These two unique properties allow shape memory alloys to have extensive applications such as prosthetic hand or active bending catheter in biomedical engineering (Cismasiu 2010). In non-medical applications, SMAs can be used as couplings and fasteners (Humbeeck 1999), tendons in structures (Song et al. 2006), actuators (Mammano and Dragoni 2011), micro actuators (Reynaerts et al. 1999), or mini actuators (Nespoli et al. 2010). Moreover, they have the potential to be used as kernel components for seismic protection devices (Dolce and Cardone 2001).

Due to the wide applications of SMA wires, several 1-D constitutive laws have been developed to study the thermomechanical behaviors of shape memory alloys. The earliest models are based on phenomenological approaches. Tanaka et al. (1982, 1986) introduced martensitic volume fraction as an internal variable and used an exponential form for kinetic

laws to calculate the amount of the martensitic volume fraction. Liang and Rogers (1990) utilized the initial martensitic volume fraction in their kinetics laws to consider the loading history in the pseudoelastic response of an SMA. Brinson (1993, 1996) divided the martensitic volume fraction into temperature- and stress-induced parts to study shape memory effect as well as pseudoelasticity.

In the existing models, it is assumed that transformation temperatures and loading history are independent. However, Buravalla and Khandelwal (2011) carried out experiments and reported different findings. In their experiments, during reverse transformation (M to A), an SMA is arrested at a temperature between  $A_s$  and  $A_f$  (in this paper, this temperature is denoted by  $A^*$ ). Afterward, the specimen is cooled to a temperature less than  $A_s$  but greater than  $M_s$ . In the subsequent heating cycle, it was observed that transformation does not start at  $A_s$ ; rather, it starts almost at the arrested temperature  $A^*$ . Similarly, for any interruption during forward transformation (A to M), a change in the martensite start temperature is observed. Moreover, if the latter heating cycle continues to a temperature above  $A_s$ , the reverse transformation does not start at  $A_s$ , but it starts at a greater temperature. Buravalla and Khandelwal (2011) realized similar phenomena in the presence of stress as well. They found empirical strain-temperature responses at a constant stress and showed that, after any interruptions during phase transformation, the subsequent transformation begins at the arrested temperature. According to these findings, it can be concluded that transformation start conditions are influenced by loading history. These results are all different from the above-mentioned assumptions made in the existing constitutive models including those proposed by Brinson (1993, 1996) and Liang and Rogers (1990).

Bekker and Brinson (1997, 1998) introduced switching points on a stress-temperature loading path in phase diagram at which martensitic volume fraction starts to change. It is expressed

that phase transformation continues as long as the projection of loading path on the normal direction of the phase diagram is a positive value. By this approach, they added a new condition to the kinetic laws for predicting the beginning of phase transformation under any arbitrary loadings. Based on this model, Buravalla and Khandelwal (2011) considered a set of projection parameters and stated that, after any interruption during phase transformation, a new transformation starts when the new projection at new switching point is smaller than the minimum of the former projection parameters in the set. This new assumption is added to Brinson model as another necessary condition for the beginning of transformations. However, this model cannot predict the shifts in  $A_s$  due to the existence of loading history. Jiang et al. (2012) carried out strain-temperature experiments in which interruptions were imposed before transformations were complete. They showed that, after any interruption, new transformation does not start at the beginning of the last one. Banerjee (2012) used both Tanaka equations (1982, 1986) and Bekker and Brinson approach (1997, 1998) to propose an algorithm for the programming of SMA wires as actuators under any arbitrary loading.

In this article, since the goal is to introduce an enhanced constitutive model for phase transformation in shape memory alloys in the simplest form, the Liang and Rogers model (1990) is used. Special heating-cooling cycles are first studied to show that initial martensitic volume fraction affects transformation start conditions. Such effects are also shown to exist in the presence of stress by carrying out simple tensile tests on Nitinol wires. Accordingly, a phenomenological approach is applied to obtain enhanced transformation start conditions as well as a new constitutive model for pseudoelasticity in the simplest form. Liang and Rogers phase diagram is generalized to transformation surfaces in which loading history is considered as one of the main parameters affecting the transformation start conditions. Moreover, history-dependent transformation start temperatures are obtained by using the present approach. This enhanced model is also derived in a continuum framework. Numerical

results are compared with the obtained experimental findings for simple tensile test of a Nitinol wire with some interruptions during unloading. A tensile stress-strain response containing several interruptions during loading, a strain-temperature response at a constant stress, and DSC results with some interruptions, done by Buravalla and Khandelwal (2011), are also compared with the predictions of the newly proposed model. A good agreement is shown to exist between the numerical and empirical results indicating the validity of the present model.

## 2. Effect of initial martensitic volume fraction on the transformation start conditions.

In order to propose an enhanced constitutive model for phase transformation in SMAs in a simple form and to examine the effects of loading history on transformation start conditions, Liang and Rogers model (1990) is considered. Referring to the phase diagram shown in Fig. 1, Liang and Rogers kinetic law for the martensitic volume fraction  $\xi$  is:

$$\left\{ \begin{array}{l} \xi = \frac{1 - \xi_0}{2} \cos \left\{ a_M \left( T - M_f - \frac{\sigma}{C_M} \right) \right\} + \frac{1 + \xi_0}{2} ; \quad A \text{ to } M \\ \quad C_M(T - M_s) < \sigma < C_M(T - M_f) \\ \xi = \frac{\xi_0}{2} \left\{ \cos \left\{ a_A \left( T - A_s - \frac{\sigma}{C_A} \right) \right\} + 1 \right\} ; \quad M \text{ to } A \\ \quad C_A(T - A_f) < \sigma < C_A(T - A_s) \end{array} \right. \quad (1)$$

where  $\xi_0$  is initial martensitic volume fraction prior to the current transformation,  $C_M$  and  $C_A$  are respectively slopes of the forward and reverse transformation strips, and the parameters  $a_M$  and  $a_A$  are defined as  $a_M = \frac{\pi}{M_s - M_f}$  and  $a_A = \frac{\pi}{A_f - A_s}$ .

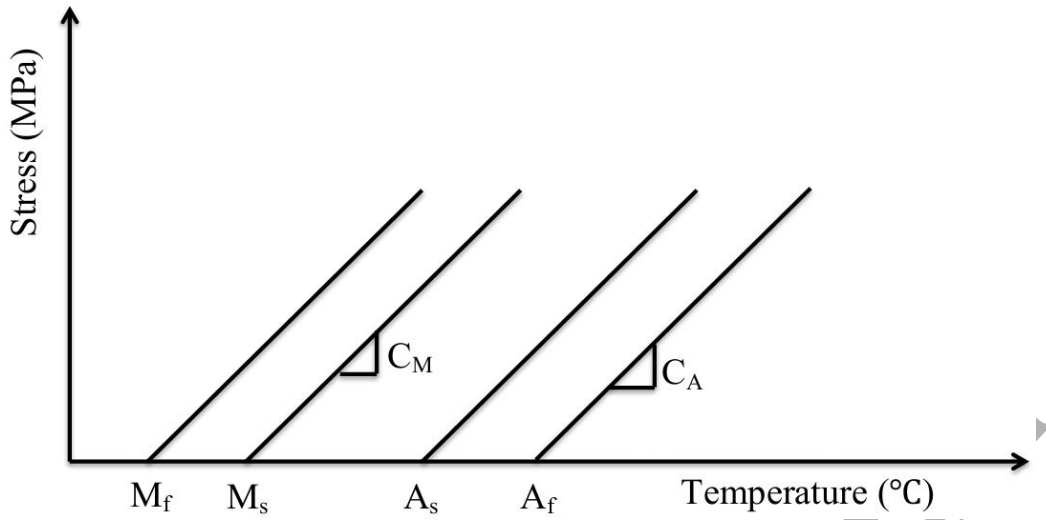
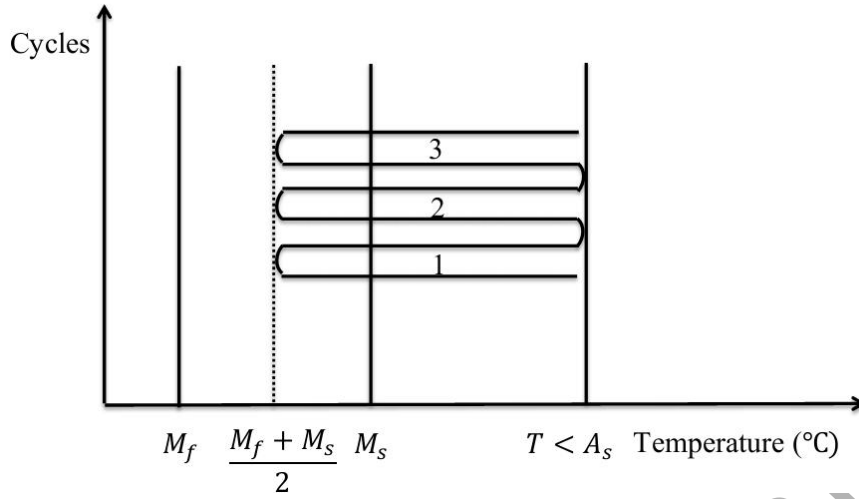
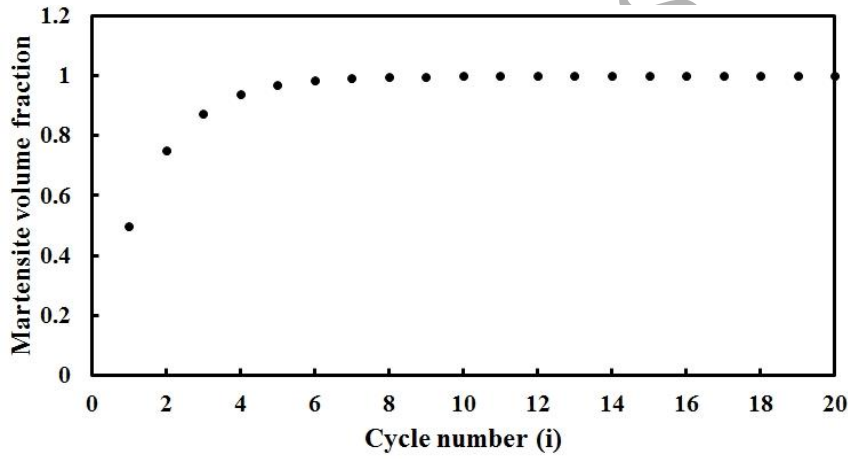


Fig. 1. Stress-temperature phase diagram in Liang and Rogers model

It is assumed in Eq. (1) that transformation start conditions and loading history are independent. Accordingly, if austenite is cooled to the temperature of  $\frac{M_s+M_f}{2}$  then heated to a temperature above  $M_s$  (but below  $A_s$ ) followed by cooling again until  $\frac{M_s+M_f}{2}$ , a new transformation still begins in  $M_s$  regardless of the thermal loading history. If this cooling-heating cycle is successively repeated as shown in Fig. 2(a), the martensitic volume fraction at the end of each cycle increases as shown in Fig. 2(b). It is seen that the amount of martensitic volume fraction reaches 1 after around 8 cycles without crossing  $M_f$ . This paradox is observed since the amount of martensitic volume fraction at the end of each cycle becomes the initial martensitic volume fraction for the next one. Additionally, it is assumed that transformation begins at  $M_s$  regardless of the thermal loading history and that the amount of martensitic volume fraction is dependent on  $\xi_0$ .



(a)

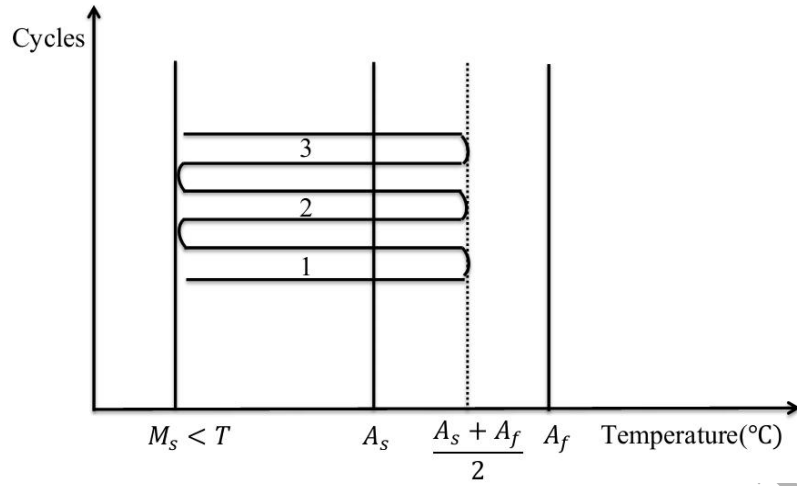


(b)

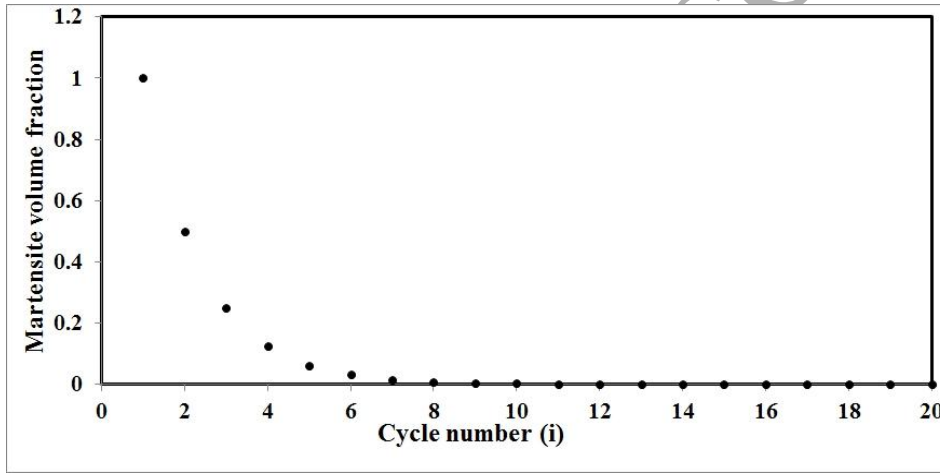
Fig. 2. (a) Schematic of the first 3 successive cooling-heating cycles at zero stress for A to M transformation. (b) Variations of martensitic volume fraction at the end of each cycle.

The same procedure can be considered for reverse transformation as well. The schematic diagram for heating-cooling cycles between a temperature greater than  $M_s$  (but below  $A_s$ ) and  $\frac{A_s + A_f}{2}$  is shown in Fig. 3(a), and variations of martensitic volume fraction are shown in Fig. 3(b). Again, it is seen that the material reaches the full austenite phase at a temperature less than  $A_f$ .





(a)



(b)

Fig. 3. (a) Schematic of the first 3 successive heating-cooling cycles at zero stress for M to A transformation. (b) Variations of martensitic volume fraction at the end of each cycle.

Reasoning behind these behaviors can be stated according to the fact that transformation start conditions and loading history in such models are independent.

### 3. An improved model.

In this section, by using a phenomenological approach, an enhanced model in the simplest explicit form is first presented. Then the proposed model is shown to be consistent with the

theory of continuum mechanics by using the continuum-based constitutive model presented by Boyd and Lagoudas (1996).

### 3.1. Phenomenological approach.

In order to examine the effects of loading history on the forward transformation start conditions, a quasi-static isothermal simple tensile test was performed on a Nitinol wire. An electromechanical testing machine (Santam STM-50) equipped with temperature-controlled environmental chamber (Applied Test Systems) was employed for the mechanical tests. A pseudoelastic wire with the diameter and length of  $d = 1$  mm and  $L = 15.5$  mm was used for tensile tests. To stabilize the stress–strain behavior of the specimen, a series of 30 tensile loading/unloading cycles was conducted at the strain rate of 0.0002/s and the ambient temperature of 20 °C. It should be noted that temperature of an SMA varies during forward as well as backward transformation especially at high strain rates (Shaw and Kyriakides, 1998; Kadkhodaei et al., 2007; Bechle and Kyriakides, 2014; Reedlunn et al. 2013 a and b; and Reedlunn et al., 2014). However, according to the available findings on the utilized NiTi wire (Kamrani and Kadkhodaei, 2015; Zare et al. 2015), the applied strain rate of 0.0002/s is reasonably considered to be low enough to maintain isothermal conditions in the experiment. In other words, no temperature variation is assumed for the specimen. The material parameters of the specimen are listed in table 1. In this table,  $E_M$  and  $E_A$  are respectively the elastic moduli of martensite and austenite.

Table 1. Material parameters of the specimen used for experiments shown in Figs. 4, 5 and 11

(Mohagheghian 2009)

$M_s$	-45°C
$M_f$	-50°C

$A_s$	$-1^{\circ}\text{C}$
$A_f$	$15^{\circ}\text{C}$
$C_M$	$6 \frac{\text{MPa}}{^{\circ}\text{C}}$
$C_A$	$5.6 \frac{\text{MPa}}{^{\circ}\text{C}}$
$E_M$	$20 \text{ GPa}$
$E_A$	$37 \text{ GPa}$

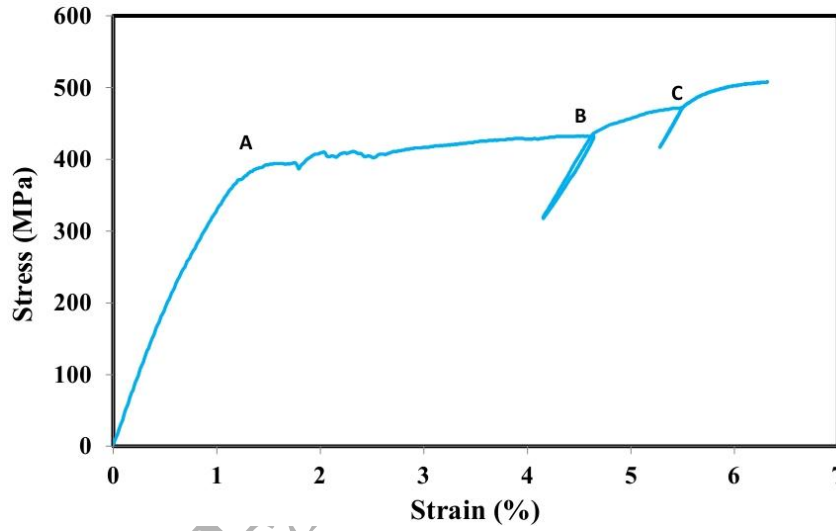


Fig. 4. Simple tensile experiment at 20 °C for examining the effect of  $\xi_0$  on the start of forward transformations

Fig. 4 shows the stress-strain response of the SMA wire with two interruptions, which are applied during the forward transformation at two different points B and C. For each interruption, the wire is partially unloaded and loaded again. In the first loading path, forward transformation begins at point A where stress equals  $C_M(T - M_s)$  according to Eq. (1). However, when transformation is arrested at point B, partial unloading causes the following transformation in the subsequent loading to begin again at the stress level of point B not A. The same behavior is seen for another interruption at point C. This phenomenon is the same

as the so-called strain hardening effect in the slip theory of plasticity according to which, after an elastic unloading, the inelastic response of a material begins at the same point where unloading was applied. In shape memory alloys, this behavior is named "arrest point memory effect" (Jiang et al. 2012).

According to the above-mentioned experimental finding, for any interruption during forward transformation, the subsequent transformation starts when stress reaches the conditions of the arrested point. In other words, in the loading parts of stress-strain diagram, the following conditions hold true for the two adjacent points to an interruption:

$$\begin{cases} \varepsilon_i = \varepsilon_n \\ \sigma_i = \sigma_n \\ \sigma_n > C_M(T - M_s) \end{cases} \quad (2)$$

In this Eq.  $\sigma$  and  $\varepsilon$  are stress and total strain, respectively. The subscripts  $i$  and  $n$  refer to the quantities right at the point where the interruption is imposed and right at the point where the subsequent transformation resumes after the interruption, respectively. Total strains are:

$$\begin{cases} \varepsilon_i = \frac{\sigma_i}{E} + H\xi_i \\ \varepsilon_n = \frac{\sigma_n}{E} + H\xi_n \end{cases} \quad (3)$$

in which  $\xi_i$  denotes the final amount of  $\xi$  at the point where transformation is arrested, and  $\xi_n$  is the martensitic volume fraction at the beginning of the subsequent transformation after interruption.  $H$  is the maximum recoverable strain. Referring to Eq. (1), the amount of  $\xi_n$  is calculated by:

$$\xi_n = \frac{1 - \xi_0}{2} \cos \left\{ a_M \left( T - M_f - \frac{\sigma_n}{C_M} \right) \right\} + \frac{1 + \xi_0}{2} \quad ; \quad A \text{ to } M \quad (4)$$

where  $\xi_0$  is the initial martensitic volume fraction prior to the beginning of the subsequent transformation. Given the fact that only elastic interruptions are considered here, it can be

concluded that the amount of  $\xi_0$  is the final amount of martensitic volume fraction right at the point where the interruption is applied. In other words:

$$\xi_i = \xi_0 \quad (5)$$

This equation states that the last amount of martensitic volume fraction becomes the initial martensitic volume fraction for the subsequent transformation (which is going to be used in Eq. (1) or (4)).

According to Fig. 4, for any interruption, slope of the stress-strain curve during the partial elastic unloading is the same as that during the subsequent elastic loading. Based on the Eq.

(2)  $\sigma_i = \sigma_n$ , this means that the elastic parts of the total strains  $\varepsilon_i$  and  $\varepsilon_n$  are equal i.e.  $\frac{\sigma_i}{E} = \frac{\sigma_n}{E}$ . Consequently, substitution of Eq. (3) into (2) yields:

$$\begin{aligned} \varepsilon_i &= \varepsilon_n \\ \Rightarrow \frac{\sigma_i}{E} + H\xi_i &= \frac{\sigma_n}{E} + H\xi_n \\ \Rightarrow H\xi_i &= H\xi_n \\ \Rightarrow \xi_i &= \xi_n \end{aligned} \quad (6)$$

Considering Eqs. (5) and (6), at the beginning of the subsequent transformation, the amount of  $\xi_n$  is equal to  $\xi_0$ :

$$\xi_0 = \xi_n \quad (7)$$

The transformation start condition can be determined by solving Eq. (7). Two distinct assumptions can be made regarding the relation between  $\xi$  and  $\xi_0$ . First, the amount of  $\xi_n$  depends on the amount of  $\xi_0$ . In other word, it is necessary to know the amount of  $\xi_0$  to determine  $\xi_n$  as it is shown in Eq. (4). Second, these two quantities are independent, so it is not necessary to know the amount of  $\xi_0$  to calculate  $\xi_n$ . Therefore, either one of the

following two formulae may be considered to calculate the amount of the martensitic volume fraction:

$$\xi_n = f(\xi_0) \quad (8)$$

or

$$\xi_n \neq f(\xi_0) \quad (9)$$

In fact, Eq. (8) states that the amount of  $\xi_n$  depends on  $\xi_0$  i.e. is a function of  $\xi_0$ . But Eq. (9) can be interpreted that the amounts of  $\xi_n$  and  $\xi_0$  are independent. Right at the interruption, if Eq. (8) is considered to be valid, substitution of  $\xi_0$  instead of  $\xi_n$  (referring to Eq. (7)) into Eq. (4) yields:

$$\begin{aligned} \xi_0 &= \xi_n \\ \Rightarrow \xi_0 &= \frac{1 - \xi_0}{2} \cos \left\{ a_M \left( T - M_f - \frac{\sigma_n}{C_M} \right) \right\} + \frac{1 + \xi_0}{2} \\ \Rightarrow \cos \left\{ a_M \left( T - M_f - \frac{\sigma_n}{C_M} \right) \right\} &= -1 \\ \Rightarrow \sigma_n &= C_M(T - M_s) \end{aligned} \quad (10)$$

This result is in contrast with both the experimental findings and the last condition in Eq. (2). Accordingly, assuming any dependence between  $\xi_n$  and  $\xi_0$  yields a contradictory result. This inconsistency shows that the amount of martensitic volume fraction and initial martensitic volume fraction are independent. Consequently, the second assumption stated in Eq. (9) should be employed. In this case, using Eq. (1) (or Eq. (4) for the forward transformation), the amount of initial martensitic volume fraction may be taken zero to satisfy the assumption that  $\xi_n$  and  $\xi_0$  are independent. By doing the similar procedure, as that employed for obtaining Eq. (10), it can be found that:

$$\xi_0 = \xi_n \quad (11)$$

$$\Rightarrow \xi_0 = \frac{1}{2} \cos \left\{ a_M \left( T - M_f - \frac{\sigma_n}{C_M} \right) \right\} + \frac{1}{2}$$

$$\Rightarrow \sigma_n = C_M(T - M_f) - \frac{C_M}{a_M} \cos^{-1}(2\xi_0 - 1)$$

Substitution of different amounts of  $\xi_i = \xi_0 \neq 0$  (referring to Eq. (5)) for each interruption into Eq. (11) shows that:

$$\sigma_i = \sigma_n > C_M(T - M_s) \quad (12)$$

Eq. (12) is indicative of the fact that the amount of stress, where new transformation resumes, is equal to the amount of stress at which transformation was arrested. It also shows that the amount of  $\xi_0$  only affects the transformation start condition. Therefore, the second assumption on the relation between  $\xi_n$  and  $\xi_0$  (Eq. (9)) is true emphasizing the fact that  $\xi_n$  and  $\xi_0$  are independent. If  $\xi_0 = 0$ , then  $\sigma_n = C_M(T - M_s)$  which is in agreement with Liang and Rogers model. But, if  $\xi_0 \neq 0$ , transformation does not start when the applied stress equals  $C_M(T - M_s)$ .

The obtained results can be generalized for the case in which there is no interruption during forward transformation. Consequently, for forward transformation, a new formula to calculate the amount of martensitic volume fraction with its transformation conditions can be stated as:

$$\begin{cases} \xi = \frac{1}{2} \cos \left\{ a_M \left( T - M_f - \frac{\sigma}{C_M} \right) \right\} + \frac{1}{2} & ; \quad A \text{ to } M \\ C_M(T - M_f) - \frac{C_M}{a_M} \cos^{-1}(2\xi_0 - 1) \leq \sigma \leq C_M(T - M_f) \end{cases} \quad (13)$$

In fact, the imposed elastic interruptions here are studied just to develop the enhanced relations above. This phenomenon can be seen for the reverse transformation as well. As shown in Fig. 5, another simple tensile test is carried out on the same material studied in Fig. 4, and two interruptions whose stress levels are less than  $C_A(T - A_s)$  are applied at points A

and D during reverse transformation. These interruptions are stopped at points B and C where stress levels are less than  $C_M(T - M_s)$ . As it is seen, after each interruption, transformation begins when stress reaches the arrested point. This again shows the so-called “arrest point memory effect” (Jiang et al., 2012). It should be noted that inhomogeneous deformations, which inherently occur in tensile loading/unloading of an SMA (Hallai and Kyriakides ,2014, Reedlunn et al. 2014, Bechle and Kyriakides, 2014, and Reedlunn et al. 2013a and b), are more evident in Fig. 5 in comparison to Fig. 4. Consequently, the "arrest point memory effect" is clearer in Fig. 4 than in Fig. 5. Such unstable material responses are not taken into account in the present study.

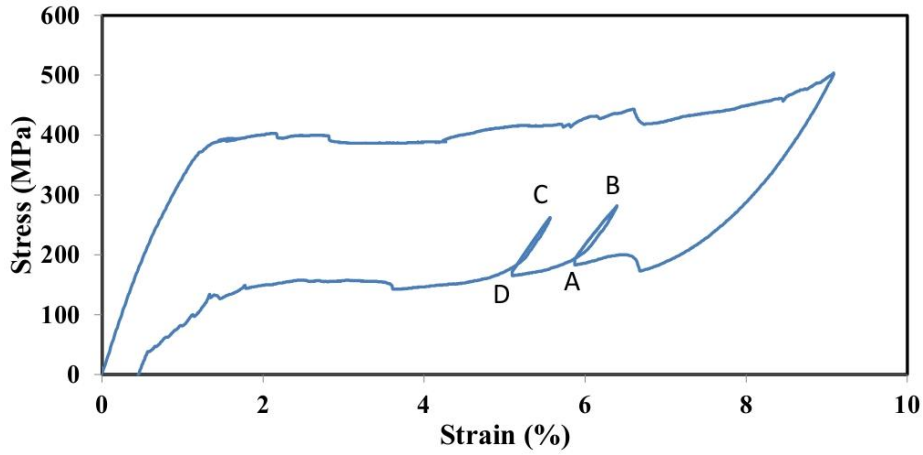


Fig. 5. Simple tensile experiment for examining the effect of initial martensitic volume fraction on the start of reverse transformations at 20 °C.

By performing the similar procedure as that done to obtain Eqs. (11) and (13), the reverse transformation start condition can be determined as:

$$\sigma_n = C_A(T - A_s) - \frac{C_A}{a_A} \cos^{-1}(2\xi_0 - 1) \quad (14)$$

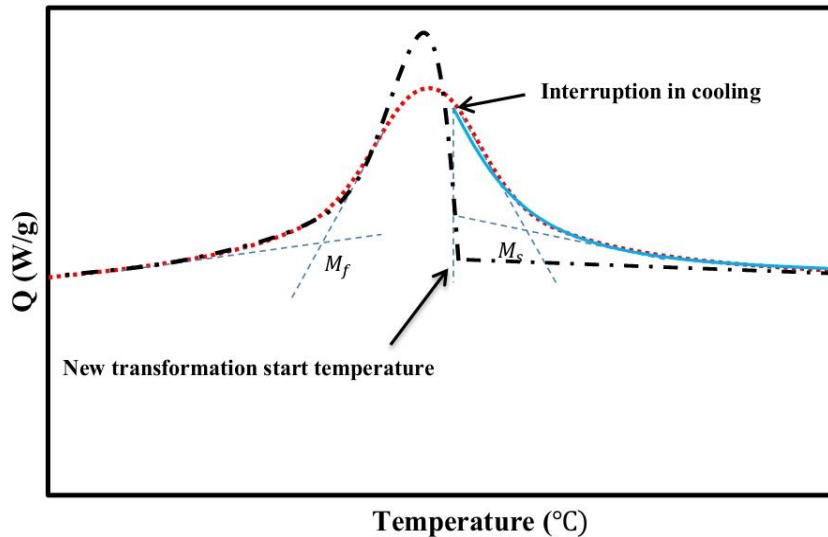
In other words, after any interruption during unloading, in the subsequent unloading, the reverse transformation resumes when the amount of stress reaches  $\sigma_n$ . Referring to the discussion provided for Eq. (13), Eq. (14) can be generalized for martensite to austenite



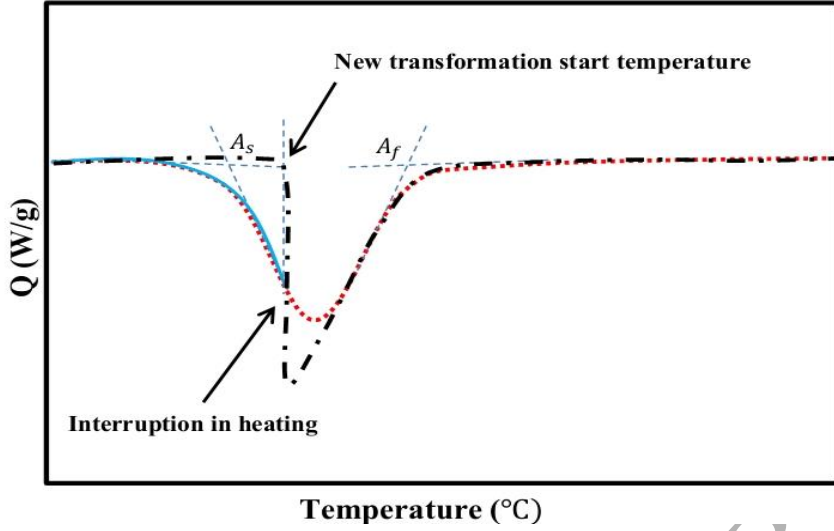
transformation . Accordingly, for reverse transformation, the new formula to determine the amount of martensitic volume fraction with its transformation start condition can be brought as:

$$\begin{cases} \xi = \frac{1}{2} \left\{ \cos \left\{ a_A \left( T - A_s - \frac{\sigma}{C_A} \right) \right\} + 1 \right\} ; & M \text{ to } A \\ C_A(T - A_f) \leq \sigma \leq C_A(T - A_s) - \frac{C_A}{a_A} \cos^{-1}(2\xi_0 - 1) \end{cases} \quad (15)$$

Buravalla and Khandelwal (2011) showed that, for any interruption during either forward or reverse transformation in DSC tests, the subsequent transformation will resume when temperature reaches the arrested point. The schematic of their DSC tests are shown in Figs. 6 (a) and (b). In these figures, the dotted lines indicate complete cooling/heating cycles. The solid lines belong to incomplete cycles where an interruption occurs, and the dash-dot lines show the subsequent cooling/heating cycle after the interruption. The dashed lines are tangent lines using which the transformation temperatures are estimated. As is seen, for both heating and cooling cycles, new transformation start temperature coincides with the arrested temperature.



(a)



(b)

Fig. 6. Schematic of DSC results (Buravalla and Khandelwal 2011) for: (a) forward transformation with an interruption during cooling cycle, (b) reverse transformation with an interruption during heating cycle

The history-dependent transformation start temperature can be determined by setting  $\sigma_n = 0$  into Eqs. (11) and (14) as:

$$\begin{cases} M_s^{\xi_0} = M_f + \frac{1}{a_M} \cos^{-1}(2\xi_0 - 1) = M_s - \frac{1}{a_M} [\pi - \cos^{-1}(2\xi_0 - 1)] \\ A_s^{\xi_0} = A_s + \frac{1}{a_A} \cos^{-1}(2\xi_0 - 1) = A_f - \frac{1}{a_A} [\pi - \cos^{-1}(2\xi_0 - 1)] \end{cases} \quad (16)$$

The notations  $M_s^{\xi_0}$  and  $A_s^{\xi_0}$  refer to the temperature in which forward and reverse transformation starts for a particular amount of  $\xi_0$ , respectively. In forward transformation when  $\xi_0 = 0$ ,  $M_s^{\xi_0}$  is equal to  $M_s$ . When  $\xi_0 = 1$ ,  $M_s^{\xi_0}$  is equal to  $M_f$ . For reverse transformation, similar results are obtained.

In the following section, the newly proposed equations are proved to be consistent with theory of continuum mechanics by using the continuum-based constitutive model presented by Boyd and Lagoudas (1996).

### 3.2. Continuum-based approach

Boyd and Lagoudas (1996) introduced a continuum-based constitutive model to model pseudoelastic behavior in shape memory alloys. In the two following subsections, this approach is briefly reviewed and the present phenomenological approach is shown to be consistent with this method.

#### 3.2.1. A brief review on Boyd and Lagoudas model.

The explicit form of Gibbs free energy (Boyd and Lagoudas 1996; Lagoudas 2008, 2012) is introduced as:

$$G(\boldsymbol{\sigma}, T, \xi, \boldsymbol{\varepsilon}^t) = -\frac{1}{2\rho} \boldsymbol{\sigma} : \mathbf{S} : \boldsymbol{\sigma} - \frac{1}{\rho} \boldsymbol{\sigma} : [\boldsymbol{\alpha}(T - T_0) + \boldsymbol{\varepsilon}^t] + c \left[ (T - T_0) - T \ln \left( \frac{T}{T_0} \right) \right] - s_0 T + u_0 + \frac{1}{\rho} f(\xi) \quad (17)$$

in which (Lagoudas 2008):

$$\begin{cases} \mathbf{S}(\xi) = \mathbf{S}^A + \xi(\mathbf{S}^M - \mathbf{S}^A) = \mathbf{S}^A + \xi \Delta \mathbf{S} \\ \boldsymbol{\alpha}(\xi) = \boldsymbol{\alpha}^A + \xi(\boldsymbol{\alpha}^M - \boldsymbol{\alpha}^A) = \boldsymbol{\alpha}^A + \xi \Delta \boldsymbol{\alpha} \\ u_0(\xi) = u_0^A + \xi(u_0^M - u_0^A) = u_0^A + \xi \Delta u_0 \\ s_0(\xi) = s_0^A + \xi(s_0^M - s_0^A) = s_0^A + \xi \Delta s_0 \\ c(\xi) = c^A + \xi(c^M - c^A) = c^A + \xi \Delta c \end{cases} \quad (18)$$

where  $\boldsymbol{\sigma}$  is stress tensor,  $\boldsymbol{\varepsilon}^t$  is transformation strain tensor,  $\mathbf{S}$  is the fourth-order compliance tensor,  $\boldsymbol{\alpha}$  is the second-order effective thermal expansion tensor,  $T$  is temperature.  $T_0$ ,  $u_0$ ,  $s_0$ ,  $\rho$  and  $c$  are reference temperature, specific internal energy at the reference state, specific entropy at the reference state, density and specific heat, respectively. Superscripts A and M in Eq. (18) refer to austenite and martensite phases, respectively. The function  $f(\xi)$  is a transformation hardening function which plays an important role in this model making it capable of predicting the SMAs' pseudoelastic response.

By using Legendre Transformation rule (Lagoudas 2008), Gibbs free energy is related to internal energy as:

$$G = u - \frac{1}{\rho} \boldsymbol{\sigma} : \boldsymbol{\varepsilon} - sT \quad (19)$$

in which  $u$  is the specific internal energy. By this rule, Gibbs free energy can be used in the first law of thermodynamic. The first law of thermodynamic is:

$$\rho \dot{u} = \boldsymbol{\sigma} : \dot{\boldsymbol{\varepsilon}} - \text{div}(\mathbf{q}) + \rho r \quad (20)$$

where  $r$  is heat source and  $\mathbf{q}$  is heat flux. By substituting Eq. (19) into (20), the first law of thermodynamics reappears as:

$$\rho \dot{G} = \rho r - \text{div}(\mathbf{q}) - \dot{\boldsymbol{\sigma}} : \boldsymbol{\varepsilon} - \rho \dot{s}T - \rho s\dot{T} \quad (21)$$

To develop an acceptable constitutive model, it should satisfy the second law of thermodynamics which is (Lagoudas 2008)

$$\rho \dot{s} + \frac{1}{T} \text{div}(\mathbf{q}) - \frac{1}{T^2} \mathbf{q} \cdot \nabla T - \frac{\rho r}{T} \geq 0 \quad (22)$$

Given the fact that the direction of  $\mathbf{q}$  and  $\nabla T$  are against each other, the term  $-\frac{1}{T^2} \mathbf{q} \cdot \nabla T$  is always greater than or equal to zero (Lagoudas 2008). As a result, the strong form of the second law of thermodynamics can be considered as (Lagoudas 2008):

$$\rho \dot{s} + \frac{1}{T} \text{div}(\mathbf{q}) - \frac{\rho r}{T} \geq 0 \quad (23)$$

Substitution of Eq. (21) into (23) yields (Lagoudas 2008):

$$-\rho \dot{G} - \dot{\boldsymbol{\sigma}} : \boldsymbol{\varepsilon} - \rho s\dot{T} \geq 0 \quad (24)$$

In which  $\dot{G}$  is:

$$\dot{G} = \frac{\partial G}{\partial \boldsymbol{\sigma}} : \dot{\boldsymbol{\sigma}} + \frac{\partial G}{\partial T} \dot{T} + \frac{\partial G}{\partial \xi} \dot{\xi} + \frac{\partial G}{\partial \boldsymbol{\varepsilon}^t} : \dot{\boldsymbol{\varepsilon}}^t \quad (25)$$

Therefore, the second law of thermodynamics is stated as (Lagoudas 2008):

$$-(\rho \frac{\partial G}{\partial \sigma} + \epsilon) : \dot{\sigma} - \rho (\frac{\partial G}{\partial T} + s) \dot{T} - \rho \frac{\partial G}{\partial \xi} \dot{\xi} - \rho \frac{\partial G}{\partial \epsilon^t} : \dot{\epsilon}^t \geq 0 \quad (26)$$

Following the Coleman and Noll procedure (1963), these relations are found (Lagoudas 2008):

$$\left\{ \begin{array}{l} \epsilon = -\rho \frac{\partial G}{\partial \sigma} = \mathbf{S} : \sigma + \alpha(T - T_0) + \epsilon^t \\ s = -\frac{\partial G}{\partial T} \\ \sigma = -\rho \frac{\partial G}{\partial \epsilon^t} \\ \sigma : \dot{\epsilon}^t + (-\rho \frac{\partial G}{\partial \xi}) \dot{\xi} \geq 0 \end{array} \right. \quad (27)$$

It is assumed (Boyd and Lagoudas 1996) that the rate of variations in the transformation strain is proportional to that of change in the martensitic volume fraction without considering the reorientation of martensitic variants. i.e.

$$\dot{\epsilon}^t = \mathbf{\Lambda} \dot{\xi} \quad (28)$$

where  $\mathbf{\Lambda}$  is transformation tensor (Boyd and Lagoudas 1996; Lagoudas et al. 2012). By substituting Eq. (28) into (27), the second law of thermodynamics (Clausius-Planck inequality) takes this form:

$$\left( \sigma : \mathbf{\Lambda} - \rho \frac{\partial G}{\partial \xi} \right) \dot{\xi} = \pi^\xi \dot{\xi} \geq 0 \quad (29)$$

The scalar  $\pi^\xi$  is called “general thermodynamic force” (Boyd and Lagoudas 1996; Lagoudas et al. 2012) which is:

$$\begin{aligned} \pi^\xi = & \sigma : \mathbf{\Lambda} + \frac{1}{2} \sigma : \Delta \mathbf{S} : \sigma + \sigma : \Delta \alpha (T - T_0) - \rho \Delta c \left[ (T - T_0) - T \ln \left( \frac{T}{T_0} \right) \right] + \rho \Delta s_0 T \\ & - \rho \Delta u_0 - \frac{\partial f}{\partial \xi} \end{aligned} \quad (30)$$

For 1-D cases, assuming that  $\Delta c = 0$ ,  $\Delta \alpha = 0$ , and  $\Delta S = 0$  (Boyd and Lagoudas, 1996; Lagoudas et al. 2012) and that the amount of  $\Lambda$  equals  $H$  (Boyd and Lagoudas, 1996; Lagoudas et al. 2012), which is the maximum transformation strain, Eq. (30) is simplified to:

$$\pi^\xi = \sigma H + \rho \Delta s_0 T - \rho \Delta u_0 - \frac{\partial f}{\partial \xi} \quad (31)$$

Transformation occurs when the general thermodynamic force reaches a threshold value called “thermodynamic driving force” (Boyd and Lagoudas, 1996; Lagoudas et al. 2012) whose amount and sign depend on the sign of  $\dot{\xi}$  in Clausius-Planck inequality. These conditions are (Boyd and Lagoudas, 1996; Lagoudas et al. 2012):

$$\pi^\xi = \begin{cases} Y & \text{for } \dot{\xi} > 0 \quad (A \text{ to } M) \\ -Y & \text{for } \dot{\xi} < 0 \quad (M \text{ to } A) \end{cases} \quad (32)$$

in which  $Y$  and  $-Y$  are the above-mentioned thermodynamic driving forces. By using different forms of the hardening function, different modes of hardening can be found (Brinson et al. 1996; Lagoudas 2008). A cosine form of the hardening function, which leads to Liang and Rogers kinetic rules, is introduced as (Lagoudas, 2008):

$$f(\xi) = \begin{cases} \int_0^\xi -\frac{\rho \Delta s_0}{a_M} [\pi - \cos^{-1}(2\xi - 1)] d\xi + (\mu_1^c + \mu_2^c) \xi; & \dot{\xi} > 0 \\ \int_0^\xi -\frac{\rho \Delta s_0}{a_A} [\pi - \cos^{-1}(2\xi - 1)] d\xi + (\mu_1^c - \mu_2^c) \xi; & \dot{\xi} < 0 \end{cases} \quad (33)$$

Substituting Eq. (33) into (31) yields:

$$\begin{cases} \sigma H + \rho \Delta s_0 T - \rho \Delta u_0 + \frac{\rho \Delta s_0}{a_M} [\pi - \cos^{-1}(2\xi - 1)] - (\mu_1^c + \mu_2^c) = Y; & \dot{\xi} > 0 \\ \sigma H + \rho \Delta s_0 T - \rho \Delta u_0 + \frac{\rho \Delta s_0}{a_A} [\pi - \cos^{-1}(2\xi - 1)] - (\mu_1^c - \mu_2^c) = -Y; & \dot{\xi} < 0 \end{cases} \quad (34)$$

In order to find the constants in Eq. (34), this equation should be calibrated. Boyd and Lagoudas introduced this procedure as (Lagoudas 2008):

1. Beginning of forward transformation ( $\dot{\xi} > 0$ ) at zero stress.

$$\pi^{\xi} = Y \quad \text{at} \quad \sigma = 0, \quad T = M_s, \quad \xi = 0 \quad (35a)$$

2. End of forward transformation ( $\dot{\xi} > 0$ ) at zero stress.

$$\pi^{\xi} = Y \quad \text{at} \quad \sigma = 0, \quad T = M_f, \quad \xi = 1 \quad (35b)$$

3. Beginning of reverse transformation ( $\dot{\xi} < 0$ ) at zero stress.

$$\pi^{\xi} = -Y \quad \text{at} \quad \sigma = 0, \quad T = A_s, \quad \xi = 1 \quad (35c)$$

4. End of reverse transformation ( $\dot{\xi} < 0$ ) at zero stress.

$$\pi^{\xi} = -Y \quad \text{at} \quad \sigma = 0, \quad T = A_f, \quad \xi = 0 \quad (35d)$$

5. continuity of Gibbs free energy

$$f(\xi = 1)|_{\dot{\xi} > 0} = f(\xi = 1)|_{\dot{\xi} < 0} \quad (35e)$$

Solution of these five equations is: (Lagoudas 2008):

$$\begin{aligned} Y &= \frac{\rho \Delta s_0}{4} [(M_s + M_f) - (A_s + A_f)] \\ a_A &= -\frac{\pi}{(A_s - A_f)} \\ a_M &= \frac{\pi}{(M_s - M_f)} \\ \mu_1^c &= \frac{1}{2} \rho \Delta s_0 (M_s + A_f) - \rho \Delta u_0 \\ \mu_2^c &= \frac{\pi}{4} \rho \Delta s_0 \left( \frac{1}{a_M} - \frac{1}{a_A} \right) \end{aligned} \quad (36)$$

Once the martensitic volume fraction is calculated, the amount of total strain is determined by:

$$\varepsilon = S\sigma + \xi H + \alpha(T - T_0) \quad (37)$$

in which the portion  $\alpha(T - T_0)$  is usually negligible compared to the other contributors to the total strain.

### 3.2.2. The newly proposed phenomenological model in the continuum framework

In this section, the newly proposed formulae are shown to be consistent with Boyd and Lagoudas approach. First, it will be shown that  $\xi$  and  $\xi_0$  are independent. Then transformation start conditions are determined. By solving Eq. (34), the kinetic laws shown in Eqs. (13) and (15) can be found. For example, here the kinetic rule for forward transformation is obtained.

$$\sigma H + \rho \Delta s_0 T - \rho \Delta u_0 + \frac{\rho \Delta s_0}{a_M} [\pi - \cos^{-1}(2\xi - 1)] - (\mu_1^c + \mu_2^c) = Y \quad (38)$$

Simplifying this equation gives

$$\begin{aligned} \frac{\rho \Delta s_0}{a_M} \cos^{-1}(2\xi - 1) &= \sigma H + \rho \Delta s_0 (T - M_f) \Rightarrow \\ \cos^{-1}(2\xi - 1) &= a_M \left[ \frac{H}{\rho \Delta s_0} \sigma + (T - M_f) \right] \Rightarrow \\ \xi &= \frac{1}{2} \cos \left( a_M \left[ \frac{H}{\rho \Delta s_0} \sigma + (T - M_f) \right] \right) + \frac{1}{2} \end{aligned} \quad (39)$$

By comparing Eqs. (39) and (13), it can be concluded that  $C_M$  and  $C_A$  are equal to  $-\frac{\rho \Delta s_0}{H}$ . Eq.

(39) also states that  $\xi$  and  $\xi_0$  are independent. For the reverse transformation, the kinetic rule can be found with the same procedure.



According to Eq. (34), the quantities  $Y$  and  $-Y$  can be determined by considering the fact that they are constant and independent of the loading history. By putting both  $\sigma$  and  $\xi$  zero in this equation and replacing  $M_s$  and  $A_f$  with temperature for cases  $\dot{\xi} > 0$  and  $\dot{\xi} < 0$ , respectively, the following relations can be obtained:

$$\begin{cases} \rho\Delta s_0 M_s - \rho\Delta u_0 - (\mu_1^c + \mu_2^c) = Y \\ \rho\Delta s_0 A_f - \rho\Delta u_0 - (\mu_1^c - \mu_2^c) = -Y \end{cases} \quad (40)$$

In the presence of loading history, where  $\xi_0$  exists, Eq. (34) reappears as:

$$\begin{cases} \sigma H + \rho\Delta s_0 T - \rho\Delta u_0 + \frac{\rho\Delta s_0}{a_M} [\pi - \cos^{-1}(2\xi_0 - 1)] - (\mu_1^c + \mu_2^c) = Y; \dot{\xi} > 0 \\ \sigma H + \rho\Delta s_0 T - \rho\Delta u_0 + \frac{\rho\Delta s_0}{a_A} [\pi - \cos^{-1}(2\xi_0 - 1)] - (\mu_1^c - \mu_2^c) = -Y; \dot{\xi} < 0 \end{cases} \quad (41)$$

By equalizing Eq.s (40) and (41), the following relations between critical stress and temperature for the beginning of transformation can be obtained:

$$\begin{cases} \sigma = C_M(T - M_s) + \frac{C_M}{a_M} [\pi - \cos^{-1}(2\xi_0 - 1)]; \dot{\xi} > 0 \\ \sigma = C_A(T - A_f) + \frac{C_A}{a_A} [\pi - \cos^{-1}(2\xi_0 - 1)]; \dot{\xi} < 0 \end{cases} \quad (42)$$

where  $C_M = C_A = -\frac{\rho\Delta s_0}{H}$ . These equations can be simplified to:

$$\begin{cases} \sigma = C_M(T - M_s) - \frac{C_M}{a_M} \cos^{-1}(2\xi_0 - 1); \dot{\xi} > 0 \\ \sigma = C_A(T - A_s) - \frac{C_A}{a_A} \cos^{-1}(2\xi_0 - 1); \dot{\xi} < 0 \end{cases} \quad (43)$$

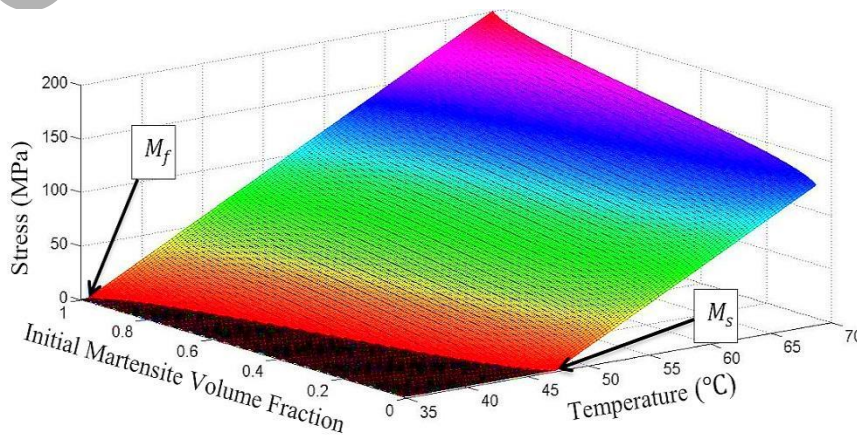
which are exactly Eqs. (11) and (14).

By setting  $\sigma = 0$  into Eq. (43), history-dependent temperatures, at which transformations resume, can be determined as:

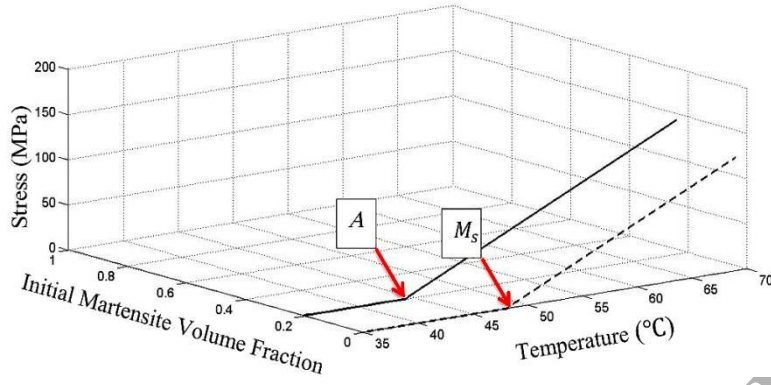
$$\begin{cases} M_s^{\xi_0} = M_f + \frac{1}{a_M} \cos^{-1}(2\xi_0 - 1) = M_s - \frac{1}{a_M} [\pi - \cos^{-1}(2\xi_0 - 1)] \\ A_s^{\xi_0} = A_s + \frac{1}{a_A} \cos^{-1}(2\xi_0 - 1) = A_f - \frac{1}{a_A} [\pi - \cos^{-1}(2\xi_0 - 1)] \end{cases} \quad (44)$$

which are exactly Eqs. (16). These equations again highlight the fact that  $\xi_0$  only affects transformation start conditions.

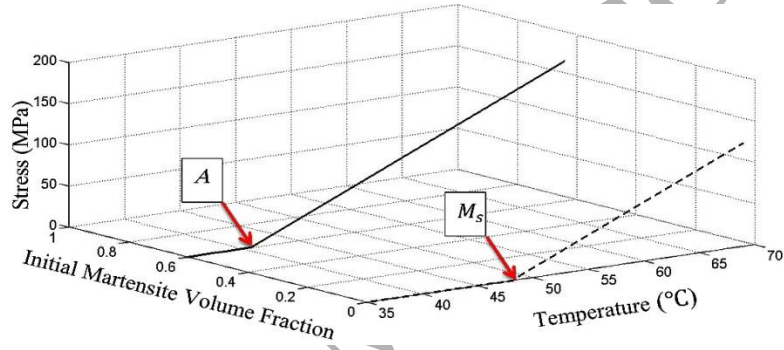
According to Eqs. (43) and (44), transformations do not start by crossing the corresponding lines in the phase diagram shown in Fig. 1 because transformation start conditions depend on the loading history. To propose a phase diagram in which the effects of loading history are taken into account, transformation surfaces in  $\sigma - T - \xi_0$  space are introduced in the present work. In other words, 2-D phase diagrams in  $\sigma - T$  space should be generalized to 3-D transformation surfaces in  $\sigma - T - \xi_0$  space in which loading history is taken into account as an extra parameter which influences the transformation start conditions. The enhanced phase diagram is shown in Figs. (7) and (8) for typical material parameters  $M_f = 35^\circ\text{C}$ ,  $M_s = 48^\circ\text{C}$ ,  $A_s = 69^\circ\text{C}$ ,  $A_f = 78^\circ\text{C}$ ,  $C_M = 6 \text{ MPa}/^\circ\text{C}$ , and  $C_A = 8 \text{ MPa}/^\circ\text{C}$  (Buravalla and Khandelwal, 2011) Figs. 7(a) and 8(a) respectively show forward and reverse transformation surfaces, and some transformation start lines for different selected amounts of  $\xi_0$  are shown in Figs. 7(b) to 7(d) and 8(b) to 8(d).



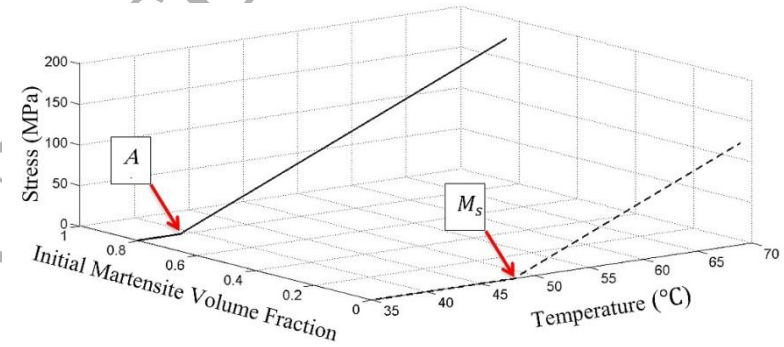
(a)



(b)



(c)

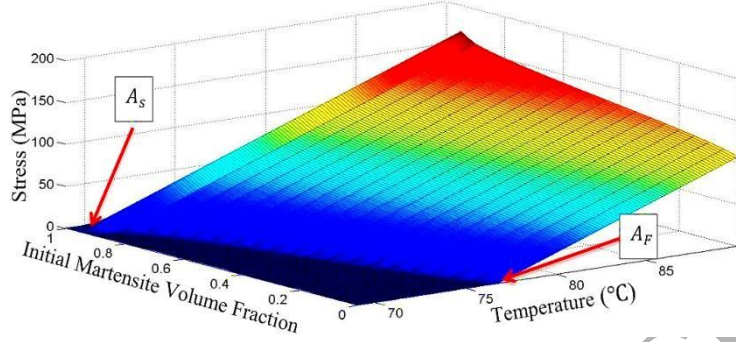


(d)

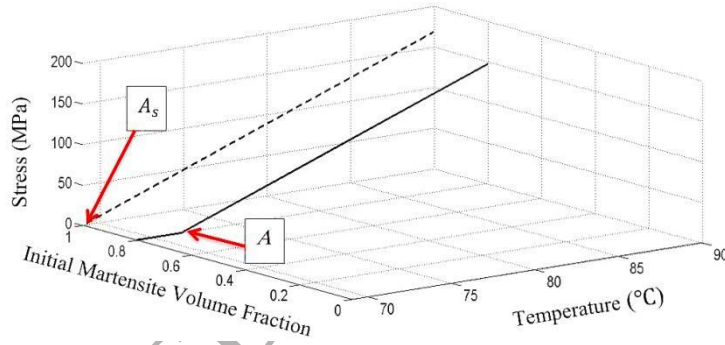
Fig. 7. The enhanced phase diagram for forward transformation (a): the surface on which transformation initiates (b): phase diagram for  $\xi_0 = 0.2$  ( $A = \begin{pmatrix} M_s^{0.2} = 44.3 \\ \xi_0 = 0.2 \\ \sigma = 0 \end{pmatrix}$ ), (c); phase diagram

for  $\xi_0 = 0.6$  ( $A = \begin{pmatrix} M_s^{0.6}=40.7 \\ \xi_0=0.6 \\ \sigma=0 \end{pmatrix}$ ), (d): phase diagram for  $\xi_0 = 0.8$  ( $A = \begin{pmatrix} M_s^{0.8}=38.9 \\ \xi_0=0.8 \\ \sigma=0 \end{pmatrix}$ ). In all figures

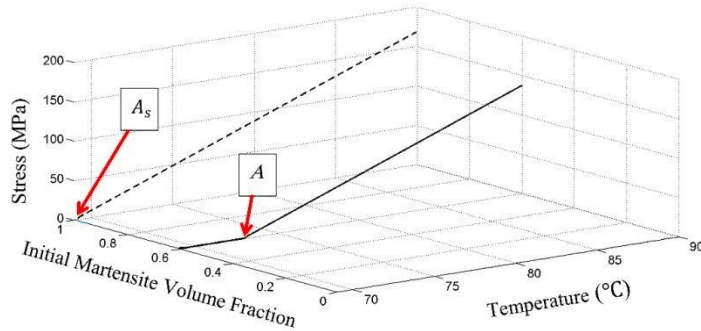
the dash-line refers to  $\xi_0=0$ .



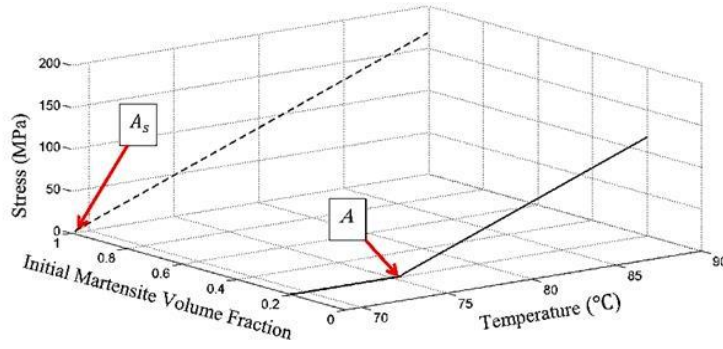
(a)



(b)



(c)



(d)

Fig. 8. The enhanced phase diagram for reverse transformation. (a) the surface on which reverse transformation initiates (b): phase diagram for  $\xi_0 = 0.8$  ( $A = \begin{pmatrix} A_s^{0.8} = 71.65 \\ \xi_0 = 0.8 \\ \sigma = 0 \end{pmatrix}$ ), (c); phase diagram for  $\xi_0 = 0.6$  ( $A = \begin{pmatrix} A_s^{0.6} = 72.85 \\ \xi_0 = 0.6 \\ \sigma = 0 \end{pmatrix}$ ), (d): phase diagram for  $\xi_0 = 0.2$  ( $A = \begin{pmatrix} A_s^{0.2} = 75.4 \\ \xi_0 = 0.2 \\ \sigma = 0 \end{pmatrix}$ ). In all figures the dash-line refers to  $\xi_0 = 1$ .

Figs. 7(a) and 8(a) indicate that, in order for transformation to occur, a loading path must be on the illustrated surfaces. Otherwise, there is no transformation and only an elastic response is observed. For instance, during forward transformation, the loading path moves on a trajectory where martensitic volume fraction increases. For any interruption during a transformation, the start condition for the subsequent one changes. In this case, the new transformation line can be determined by intersecting the transformation surface and the plane of the obtained martensitic volume fraction by Eq. (13). Moreover, after any interruption, the final amount of martensitic volume fraction appears as  $\xi_0$  for the next phase transformation. These details should be considered for reverse transformation as well.

As a summary of this section, the total strain is determined by Eq. (37) where the amount of martensitic volume fraction is calculated by Eqs. (13) and (15), and transformation start temperatures are determined by Eqs. (16).

#### 4. Results and discussion.

In this section, first, variations of the transformation start temperatures due to interruptions during cooling/heating cycles are studied, and the numerical predictions are compared with experimental ones obtained from DSC tests reported by Buravalla and Khandelwal (2011) on two different alloys with the material parameters listed in Table 2.

Table 2. Material parameters in DSC tests done by Buravalla and Khandelwal (2011)

Material id-1	Material id-2
$M_s=48^\circ\text{C}$	$M_s=60^\circ\text{C}$
$M_f=35^\circ\text{C}$	$M_f=54^\circ\text{C}$
$A_s=69^\circ\text{C}$	$A_s=70^\circ\text{C}$
$A_f=78^\circ\text{C}$	$A_f=80^\circ\text{C}$
$E_M=27.3 \text{ GPa}$	$E_M=27.3 \text{ GPa}$
$E_A=55.055 \text{ GPa}$	$E_A=55.55 \text{ GPa}$
$C_M=6 \frac{\text{MPa}}{^\circ\text{C}}$	$C_M=18 \frac{\text{MPa}}{^\circ\text{C}}$
$C_A=8 \frac{\text{MPa}}{^\circ\text{C}}$	$C_A=15 \frac{\text{MPa}}{^\circ\text{C}}$
$H=0.06$	$H=0.05$

Table 3 shows the numerical and experimental results for two DSC tests in the manner shown in Fig. 6. In this table, the first two rows indicate the case in which two different interruptions between  $M_s$  and  $M_f$  are applied during cooling (Fig. 6(a) on material id-1), and the transformation start temperature in the subsequent cooling is determined for each interruption. In the last row of this table, a comparison between the numerical and

experimental results for the case of Fig 6(b) is shown in which an interruption between  $A_s$  and  $A_f$  is applied during heating.

Table 3. Numerical and experimental results for DSC test shown in Fig. 6(a) on material id-1

Material	Experimental case shown in figure:	Arrested temperature	Subsequent start temperature (Experiment (Buravalla and Khandelwal 2011))	Subsequent start temperature (proposed model)
id-1	6(a)	45°C	45.6°C	45°C
id-1	6(a)	42°C	42.4°C	42°C
id-2	6(b)	74°C	74°C	74°C

According to Table 3, the good agreement between the numerically predicted temperatures and the empirically found ones indicates the accuracy of the proposed approach in determination of the history-dependent transformation start temperatures.

Buravalla and Khandelwal (2011) state that, if forward transformation is arrested between  $M_s$  and  $M_f$ , reverse transformation will not occur at  $A_s$ , but starts at a shifted temperature between  $A_s$  and  $A_f$ . Fig. 9 shows the numerical results of the present model for such a cooling/heating cycle (solid line) on material id-1 along with the corresponding complete transformation cycle (dot line). In the studied incomplete transformation cycle, an interruption occurs during cooling at point B. As it is seen, upon heating, reverse transformation begins at  $A_s^{\xi_0}$  in agreement with the above-mentioned statement.

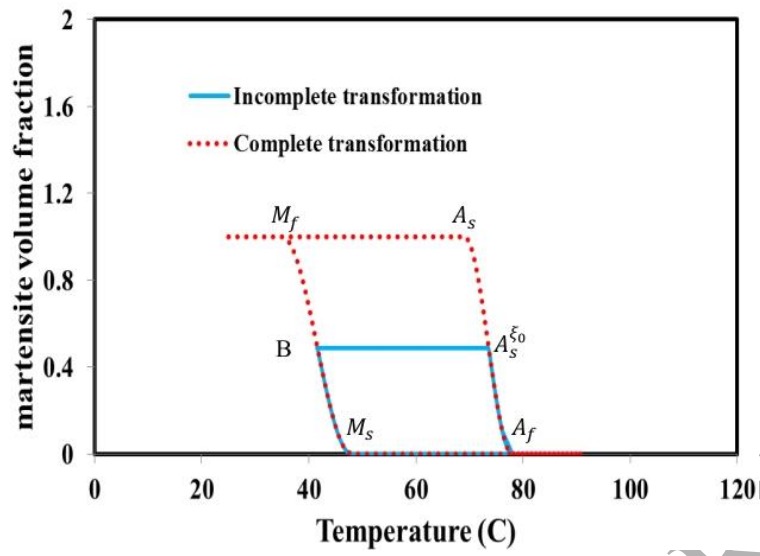
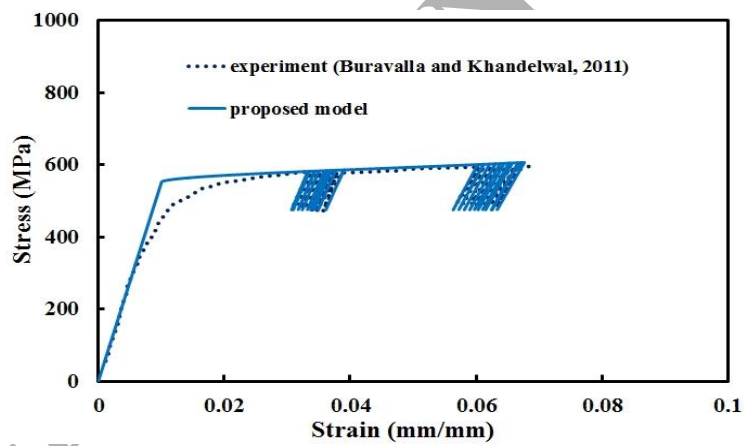
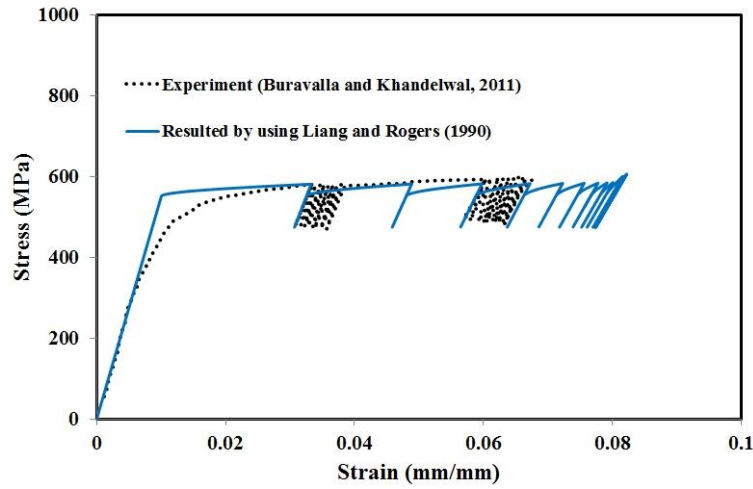


Fig. 9. Comparison between complete and incomplete cooling/heating cycles on material id-1



(a)





(b)

Fig. 10. Stress-strain response in a uniaxial loading with several interruptions at the constant temperature of 141 °C for material id-1: (a) Comparison of the present model and experiment (Buravalla and Khandelwal 2011), (b) Comparison of Liang and Rogers (1990) model and experiment (Buravalla and Khandelwal 2011)

In Fig. 10(a) and (b), stress-strain response in a uniaxial loading containing several interruptions is studied. The experimental results belong to the simple tensile test done by Buravalla and Khandelwal (2011) on material id-1. As is seen in Fig. 10(a), the numerical curve obtained from the present model reproduces the experimental one with good accuracy. However, Fig. 10(b) shows that Liang and Rogers (1990) model (just as a sample of the existing 1-D constitutive models) predicts different results than the empirical ones. Apart from differences in the critical stresses for the beginning of forward transformation, it is seen that the amount of strain between the experimental and numerical results after the first incomplete unloading is different since the interruptions are done at specified stress levels. Moreover, by gradually increasing the arrested stress, the theoretical response gradually converges to a fixed line while this is not the case for experimental findings.

In order to investigate a case where arrested stresses are more distinguishable and occur in the course of reverse transformation, a simple tensile test with two interruptions during unloading is carried out on the Nitinol wire with material parameters shown in table 1. In Fig. 11, the experimental findings are compared with the numerical results obtained by using both the newly proposed approach and Liang and Roger (1990) model. In this figure, forward transformation during loading starts at point A and finishes at Point B. The loading continues to point C, and reverse transformation starts at point D during unloading. At point E, an interruption is applied where a new loading starts and continues to point F which has a stress level lower than  $C_M(T - M_s)$ . In the subsequent unloading, both experiment and the present model show that transformation starts at point E whereas Liang and Rogers model predicts that it occurs at point H whose stress is equal to that of point D. Similar to Fig. 10(b), this difference between the results causes the amount of total strain obtained in experiment and the predicted number by the present approach to be different from those obtained by Liang and Rogers model in the second unloading after the first interruption. The second unloading continues to point G at which the second interruption is applied. Due to the differences between the amounts of strain, the same stress level of point G is seen in point I of the curve obtained by Liang and Rogers model. During the subsequent unloading, again both experiment and the present model show that the subsequent transformation resumes at the arrested point G while Liang and Rogers model predicts that it occurs at point J whose stress level is still equal to that of point D. In the third unloading, more pronounced differences are seen between the amounts of strain obtained by the two models. As described in Fig. 5, the empirically-observed inhomogeneous deformations in Fig. 11 are not considered in the present model. In other words, the proposed approach is not able to capture unstable material response, and further developments are required to resolve this limitation. The observed residual strain in the experimental response may be due to (any possible) plastic deformations

in the course of loading (Hartl and Lagoudas, 2009) or residual martensite remaining at the end of unloading (Saint-Sulpice, Arbab Chirani and Calloch 2009), but these details are not taken into account in the present approach.

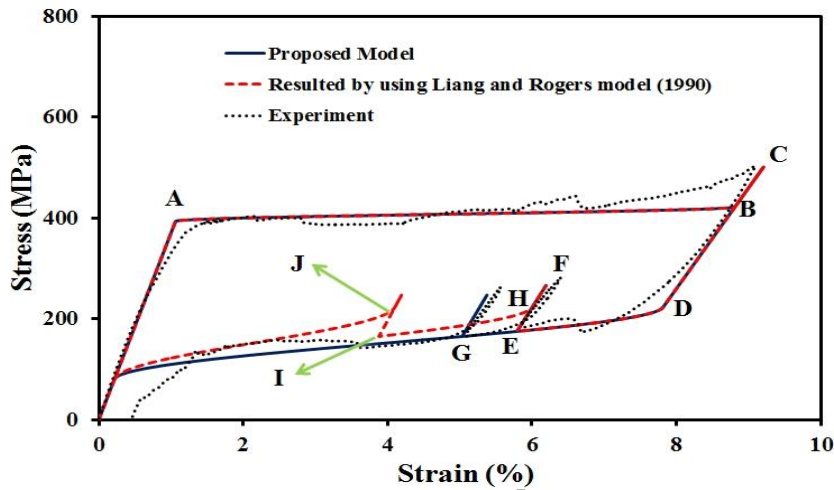
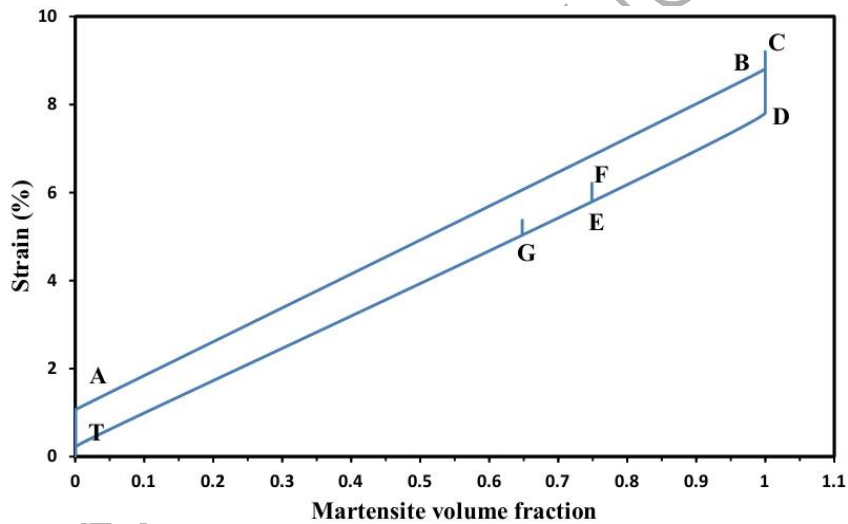


Fig. 11. Comparison between the present model (solid line), experiment (dot line), and Liang and Rogers model (dashed line) for simple tensile test with interruptions during unloading at 23°C

To better illustrate differences in the predicted strains by the both current approach and Liang and Rogers model, variations of strain with the martensitic volume fraction are shown in Fig. 12(a) and (b) for the two models. Between points A and B, where forward transformation starts and finishes, the total strain increases with increase in the martensitic volume fraction. Between points B and C, at the constant martensitic volume fraction of unity, total strain increases as a result of elastic response. During unloading, decrease in the strain is first seen at the constant martensitic volume fraction until point D followed by decline in both strain and martensitic volume fraction until point E where the first interruption occurs. Between points E and F, strain again increases at a constant martensitic volume fraction due to the elastic response during the partial loading. In Fig. 12(a), where results of the present

approach are shown, new transformation starts again at point E during the subsequent unloading. However, shown in Fig. 12(b), Liang and Rogers (1990) model predicts that the new transformation starts at point H which is not coincident with point E. At the stress level of the second interruption shown in Fig. 11, the present model predicts this interruption occurs at point G. But Liang and Rogers model yields point I whose strain and martensitic volume fraction are significantly different from those at point G. In the subsequent unloading, the present model again predicts that the new transformation begins at point G while point J is obtained by Liang and Rogers model.



(a)

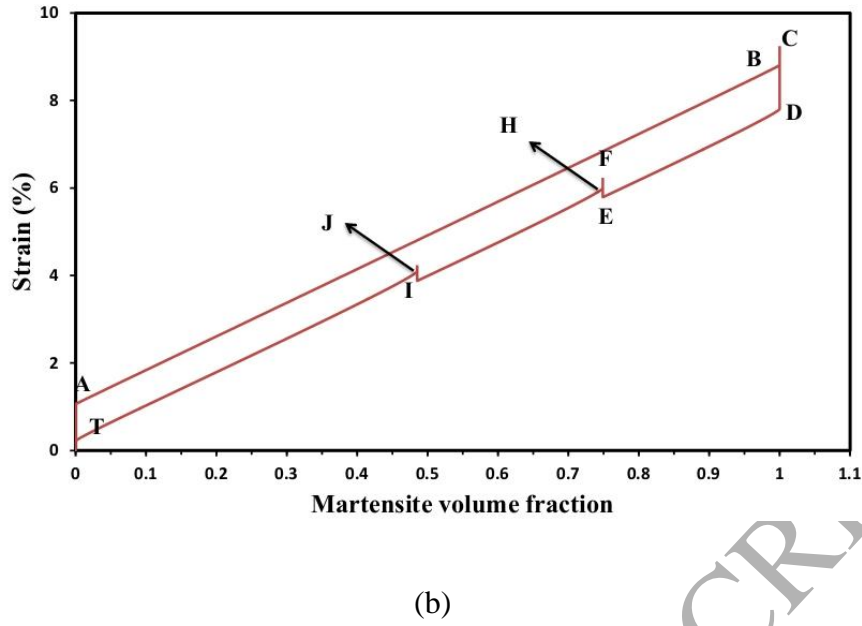


Fig. 12. Variations of strain with the martensitic volume fraction for Fig. 11: (a) Results of the proposed model, (b) Results of Liang and Rogers (1990) model.

In Fig. 13, strain-temperature response (Buravalla and Khandelwal 2011) at the constant stress of 110 MPa is compared with numerical results obtained by the newly presented model. As it is seen, an interruption is applied during cooling followed by partial heating and subsequent cooling. Again the numerical results can reproduce the experimental ones with a reasonable accuracy in that, after imposing the interruption, the subsequent transformation starts at the arrested point.

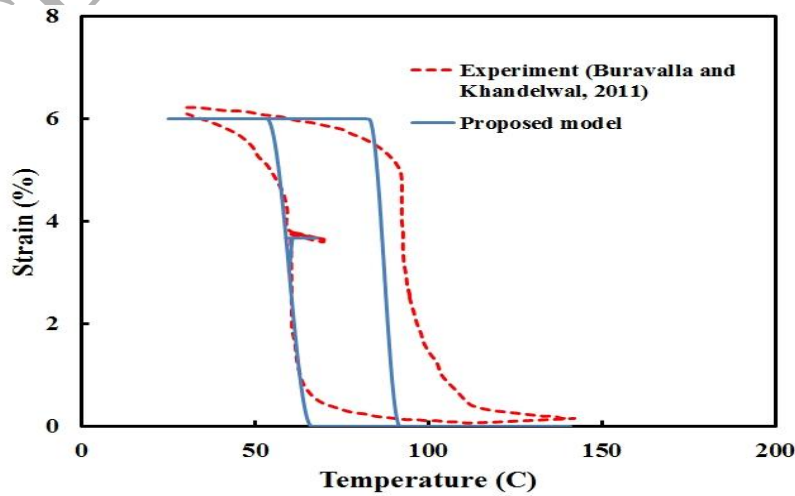


Fig. 13. Strain-temperature response at the constant stress of 110 MPa for material id-1

## 5. Conclusion

In this paper, a new one-dimensional constitutive model in the simplest form for phase transformation is proposed by using a phenomenological approach to consider the effects of loading history on the initiation of transformations in shape memory alloys. The present model is also proved to be consistent with the theory of continuum mechanics. This model introduces an enhanced phase diagram in which transformation surfaces are defined according to which A to M and M to A transformations occur. Transformation temperatures are concluded not to be fixed values but depend on heating/cooling history prior to the current transformation. Moreover, in the presence of stress, it is shown that the initial martensitic volume fraction affects the critical stresses to start transformations but does not have any influences on the amount of martensitic volume fraction. Explicit formulae for the history-dependent transformation temperatures and the martensitic volume fraction along with transformation surfaces are proposed. The present model is validated by several experimental data. Furthermore, Liang and Rogers model, as a sample of the existing 1-D constitutive equations, is compared with the present model and experiments to show the efficiency of the present work in studying pseudoelastic behavior of shape memory alloys.

## 6. Acknowledgment

Prof. Mohammad Elahinia from the University of Toledo is gratefully acknowledged for his instructive discussions throughout the present work.

## 7. References

Banerjee, A., 2012. Simulation of shape memory alloy wire actuator behavior under arbitrary thermo-mechanical loading. *Smart Mater Struct* 21 125018.

- Bechle, N. J. and Kyriakides, S. 2014. Localization in NiTi tubes under bending. *Int J Sol Struct* 51(5), 967-980.
- Bekker, A. and Brinson, L.C., 1998. Phase diagram based description of the hysteresis behavior of shape memory alloys. *Acta Mater.* 46 (10): 3649–3665.
- Bekker, A. and Brinson, L.C., 1997. Temperature-induced phase transformation in a shape memory alloy: phase diagram based description. *J Mech Phys Solids* 45 (6): 949–988.
- Boyd, J.G. and Lagoudas, D.C., 1996. A thermodynamical constitutive model for shape memory materials. Part I. The monolithic shape memory alloy. *Int J Plast* 12 (6): 805–842.
- Brinson, L.C. and Huang, M.S., 1996. Simplifications and comparisons of shape memory alloy constitutive models. *J Intell Mater Syst Struct* 7: 108-14.
- Brinson, L.C., 1993. One dimensional constitutive behavior of shape memory alloys: thermodynamical derivation with non-constant material functions and redefined martensite internal variable. *J Intell Mater Syst Struct* 4(2): 229-42.
- Buravalla, V. and Khandelwal, A., 2011. Evolution kinetics in Shape Memory Alloys under arbitrary loading: Experiments and modeling. *J Mech Mater* 43: 807-823.
- Cismasiu, C., 2010. Shape Memory Alloys. Sciyo, Rijeka, Croatia.
- Coleman, B.N. and Noll, W., 1963. The thermodynamics of elastic materials with heat conduction and viscosity. *Arch Rat Mech Anal* 13: 167–178.
- Dolce, M. and Cardone, D., 2001. Mechanical behaviour of shape memory alloys for seismic applications. 1. martensite and austenite NiTi bars subjected to torsion. *Int J Mech Sci* 43: 2631–2656.

- Hallai, J. F. and Kyriakides, S. 2013. Underlying material response for Lüders-like instabilities. *Int J Plas*, 47, 1-12.
- Hartl, D. J., and Lagoudas, D. C. 2009. Constitutive modeling and structural analysis considering simultaneous phase transformation and plastic yield in shape memory alloys. *Smart Materials and Structures*, 18(10), 104017.
- Humbeeck, J.V., 1999. Non-medical applications of shape memory alloys. *Mater Sci Eng. A*: 273 – 275, 134 – 148.
- Jiang, J., Cui, L., Zheng, Y.J., Jiang, D.Q., Liu, Z.Y. and Zhao, K., 2012. Negative thermal expansion arrest point memory effect in NiTi shape memory alloy and NbTi/TiNi composite. *Mater Sci Eng A* 549: 114-117.
- Kadkhodaei, M., Rajapakse, R. K. N. D., Mahzoon, M., & Salimi, M., 2007. Modeling of the cyclic thermomechanical response of SMA wires at different strain rates. *Smart Mater Struct*, 16(6), 2091.
- Kamrani, M., and Kadkhodaei, M. 2015. Investigation on local and global behaviors of pseudoelastic shape memory alloy wires in simple tensile test considering stress concentration of grippers. *Journal of Intelligent Material Systems and Structures*, 1045389X14566519.
- Liang, C. and Rogers, C.A., 1990. One-Dimensional Thermomechanical Constitutive relations for Shape Memory Materials. *J Intell Mater Syst Struct* 1: 207-34.
- Lagoudas, D., Hartl, D., Chemisky, Y., Machado, L. and Popov, P., 2012. Constitutive model for the numerical analysis of phase transformation in polycrystalline shape memory alloys. *Int J Plast* 32-33: 155-183.



Lagoudas, D.C., 2008. Shape Memory Alloys: Modeling and Engineering Applications. Springer, New York.

Mammano, G.S. and Dragoni, E., 2011. Increasing stroke and output force of linear shape memory actuators by elastic compensation. *Mecha* 21: 570–580.

Mohagheghian, I., 2009. Investigation on Thermomechanical Behavior of SMA wires M.Sc. Thesis, Isfahan University of Technology (in Persian).

Nespoli, A., Besseghini, S., Pittaccio, S., Villa, E. and Viscuso, S., 2010. The high potential of shape memory alloys in developing miniature mechanical devices: A review on shape memory alloy mini-actuators. *Sens Act A* 158: 149–160.

Qidwai, M.A. and Lagoudas, D.C., 2000. Numerical implementation of a shape memory alloy thermomechanical constitutive model using return map-ping algorithms. *Int J Num Meth Eng* 47: 1123–1168.

Reedlunn, B., Daly, S. and Shaw, J. 2013a. Superelastic shape memory alloy cables: Part I–isothermal tension experiments. *Int J Sol Struct* 50(20), 3009-3026.

Reedlunn, B., Daly, S. and Shaw, J. 2013b. Superelastic shape memory alloy cables: Part II–Subcomponent isothermal responses. *Int J Sol Struct*, 50(20), 3027-3044.

Reedlunn, B., Churchill, C. B., Nelson, E. E., Shaw, J. A., and Daly, S. H. 2014. Tension, compression, and bending of superelastic shape memory alloy tubes. *J Mech Phys Sol*, 63, 506-537.

Reynaerts, D., Peirs, J. and Brussel, H.V., 1999. Shape memory micro-actuation for a gastrointestinal intervention system. *Sens Act* 77: 157–166.

Saint-Sulpice, L., Chirani, S. A., and Calloch, S. 2009. A 3D super-elastic model for shape memory alloys taking into account progressive strain under cyclic loadings. *Mechanics of materials*, 41(1), 12-26.

Shaw, J.A., Kyriakides, S., “Initiation and Propagation of Localized Deformation in Elasto-Plastic Strips under Uniaxial Tension” *International Journal of Plasticity*, Vol. 13, No. 10, pp. 837-871, 1998

Song, G., Ma, N. and Li, H.N., 2006. Applications of shape memory alloys in civil structures. *Struc Eng* 28: 1266–1274.

Tanaka, K., 1986. A thermomechanical sketch of shape memory effect: one-dimensional tensile behavior. *Res Mech Int J Struct Mech Mater Sci* 18: 251-63.

Tanaka, K. and Nagaki, S., 1982. A thermomechanical description of materials with internal variables in process of phase transformation. *Ing Arch* 52: 287-99.

Zare, F., Kadkhodaei, M., and Salafian, I. 2015. Thermomechanical Modeling of Stress Relaxation in Shape Memory Alloy Wires. *Journal of Materials Engineering and Performance*, 24(4), 1763-1770.